HHS Public Access

Author manuscript

*Nat Struct Mol Biol*. Author manuscript; available in PMC 2013 August 01.

Published in final edited form as:

*Nat Struct Mol Biol*. 2013 February ; 20(2): 215–221. doi:10.1038/nsmb.2494.

# Conformational ensemble of the sodium coupled aspartate transporter

**Elka R. Georgieva**[1,2], **Peter P. Borbat**[1,2], **Christopher Ginter**[3], **Jack H. Freed**[1,2], and **Olga Boudker**[3]

[1]National Biomedical Center for Advanced ESR Technology, Cornell University, Ithaca, New York, USA

[2]Department of Chemistry and Chemical Biology, Cornell University, Ithaca, New York, USA

[3]Weill Cornell Medical College, Department of Physiology and Biophysics, New York, New York, USA

## Abstract

Sodium and aspartate symporter from *Pyrococcus horikoshii*, $Glt_{Ph}$, is a homologue of the mammalian glutamate transporters, homotrimeric integral membrane proteins controlling the neurotransmitter levels in brain synapses. These transporters function by alternating between outward and inward facing states, in which the substrate binding site is oriented toward the extracellular space and the cytoplasm, respectively. Here we employ double electron-electron resonance (DEER) spectroscopy to probe the structure and the state distribution of the subunits in the trimer within distinct hydrophobic environments of detergent micelles and lipid bilayers. Our experiments reveal a conformational ensemble of protomers sampling the outward and inward facing states with nearly equal probabilities, indicative of comparable energies, and independently of each other. On average, the distributions vary only modestly in detergent and in bilayers, but in several mutants unique conformations are stabilized by the latter.

## Introduction

Glutamate is a major excitatory neurotransmitter in the central nervous system and plays crucial roles in learning, memory formation and cognition [1]. Although glutamate is abundant in the brain, its extracellular concentration is tightly controlled to allow for neurotransmission, and abnormally elevated levels observed in several neurodegenerative diseases, ischemia and epilepsy are toxic [2]. Glutamate transporters are electrochemically driven pumps, which couple uptake of glutamate into the cytoplasm of astrocytes and



Correposndence should be addressed to O. B. (olb2003@med.cornell.edu).

**Author contributions**

E.R.G. and O.B. developed the mutation strategy for DEER and designed the molecular biology and biochemical part of the experiments. E.R.G., P.P.B. and J.H.F. designed the DEER experiments. E.R.G. performed most of the DEER experiments, protein expression and purification, and spin-labeling. C.G. carried out the mutagenesis and participated in protein expression and purification. P.P.B. performed some of the DEER measurements. E.R.G., O.B. and P.P.B. analyzed the data. O.B., E.R.G., P.P.B. and J.H.F. wrote the manuscript.

neurons to the thermodynamically downhill movements of ions [3–5]. The structural information for this family comes from the crystal structures of an archaeal homologue, $Glt_{Ph}$ [6–9], a sodium and aspartate symporter [7,10,11], which shares ~35% amino acid sequence identity with the mammalian glutamate transporters and provides a model system to study their mechanism. The crystal structures revealed a homotrimeric assembly, common for all characterized members of the family [12,13]. Each protomer harbors an independent set of aspartate (Asp) and sodium ($Na^+$) binding sites at the core of a peripherally located transport domain (Figure 1a). The central trans-membrane segments form the trimerization domain, mediating inter-subunit contacts and remaining largely unchanged during transport [8,9,14]. In contrast, transport domains show structural plasticity leading to 15 – 18 Å movements across the membrane, thereby switching the substrate and ion binding sites between the extracellular and cytoplasmic orientations, i.e. the outward and inward facing states, respectively. Two re-entrant hairpin (HP) segments of the transport domain, HP1 and 2, occlude the substrate and ions from the aqueous milieus in both states, and HP2 has been proposed to serve as an extracellular gate [7,15–17]. Asp binding and closure of the extracellular gate are thermodynamically coupled to binding of $Na^+$ ions[7]. In contrast, iosmerization between the outward and inward facing states has been proposed to occur independently of the ions, driven primarily by the thermal energy[8].

Here, we aim to gain structural information on the outward and inward facing states of $Glt_{Ph}$ and to establish their energetic relationship in two distinct hydrophobic environments, namely in detergent micelles and in lipid bilayers. In this way we begin to sketch out the energy profile of the transport cycle. Toward this end, we employ site-directed spin labeling and DEER spectroscopy to measure the distances between the paramagnetic probes. The technique provides access to distances and, importantly, distance distributions ranging from 20 to over 80 Å[18–21] and has been applied to study diverse systems, including membrane proteins within lipid bilayers[20,22–29]. Here, we have further broadened the applicability of DEER spectroscopy by extracting quantitative information on the populations and the energies of the conformational states contributing to the experimentally observed distance distributions.

We used spin-labeled cysteine mutants of $Glt_{Ph}$ for the long-range distance measurements either when the transporters were empty or loaded with $Na^+$ ions and Asp or an inhibitor. We obtained broad distance distributions, which we interpret in terms of an ensemble of the underlying inward and outward facing states, consistent with the known crystal structures. The quantitative analysis reveals that the two states are populated with almost equal probabilities under all conditions, indicating similar energies. Moreover, our data are consistent with a lack of cooperativity within the trimers, painting a picture of a system in which each protomer samples outward and inward facing conformations independently of its neighbors, regardless of whether it is loaded with the substrate or empty. On average, we find no substantial differences in either the structure or the relative energies of the outward and inward facing states in detergent micelles and in lipid bilayers. However, in several mutants, in which the spin label was placed on the interface between the transport and trimerization domains in one of the states, we saw substantial stabilization of those states in lipid but not detergent. These results suggest that the spin label participates in specific

protein interactions, and remarkably, that these interactions are more favorable when the transporter is embedded into membrane compared to detergent micelles.

## Results

### Spin labeling strategy

Isomerization of GltPh between the outward and inward facing states as seen by crystallography[6–8] involves an ~15 Å translation and a 35° rotation of the transport domains relative to the trimerization domain (Figure 1a). As a result, the inter-subunit distances between equivalent residues in the transport domains change by up to 20 Å, providing means to distinguish the states. For single cysteine mutagenesis and labeling, we selected residues that are solvent accessible in at least one of the conformations, and for which the inter-subunit distances lie between ~20 and 70 Å, most suitable for DEER analysis (Figure 1b, Supplementary Table 1). Specifically, we chose two regions distant from the substrate and ion binding sites, one on each the cytoplasmic and the extracellular side, and the third on HP2 (Figure 1c). Two residues in the trimerization domain, which is expected to remain rigid upon substrate binding or translocation, served as controls. The purified cysteine mutants were spin-labeled, and DEER measurements (Supplementary Figure 1 and Supplementary Note) were conducted either in detergent or after reconstitution into lipid bilayers.

### Structural stability of the trimerization domain

For the labeled trimerization domain mutant, K55R1 (R1 denotes a spin-labeled cysteine), the amplitude of the DEER signal at zero time in detergent was consistent with the complete spin labeling of the cysteine residues (Figure 2a, Supplementary Figure 2a and Supplementary Note). The clear oscillations in the time evolution signal indicated a narrow range of the inter-spin distances. The extracted distance distributions covered a range between 18 and 30 Å for the substrate-free apo $Glt_{Ph}$ and the transporter bound to $Na^+$ and Asp or to a transport blocker, DL-*threo*-β-bezyloxyaspartate (TBOA). Similar results were obtained in detergent and lipid. The distribution medians (Figure 2b) varied between 23 and 28 Å, in excellent agreement with the $C_\beta$-$C_\beta$ inter-protomer distances in the crystal structures of the outward and inward facing $Glt_{Ph}$ (Figure 1b and Supplementary Table 1). The distribution widths (2.8 – 4.6 Å) were similar to those obtained for soluble well-folded proteins [30–32]and likely originate mainly from the conformational flexibility of the R1 side chain.

Interestingly, similar but distinct signals were obtained for GltPh-K55R in the apo state and when bound to either Asp or TBOA, particularly in detergent. Residue 55 is at the interface of the transport and trimerization domains, and likely experiences distinct steric constraints in the outward and inward facing states, which may underlie differences in the inter-spin distances. To test this, we computed theoretical distance distributions based on energy-weighted R1 rotamer libraries generated by a modeling program MMM[33] using crystallographic structures of $Glt_{Ph}$ in the symmetric outward and inward facing states along with a model of an asymmetric trimer with two protomers in the outward and one in the inward facing state (Online Methods). Modeling suggested that R1 in position 55 was more

sterically constrained in the inward facing conformation with fewer accessible rotamers (Figure 2c and Supplementary Figure 2b). Notably, experimental distance distributions encompassed predicted features of both the outward and inward facing states, suggesting that both were populated. We obtained similar results for V216R1 mutant, located in a more flexible peripheral part of the trimerization domain. Consistently, the experimental distance distributions were broader with widths of 5.2 – 7.6 Å (Supplementary Figure 3 and Supplementary Table 1).

In order to evaluate potential contributions from the three-spin effects to the apparent distance distributions [34,35], we collected DEER data on $Glt_{Ph}$-K55R1 using pump pulses with decreasing amplitude (Supplementary Note). As expected for a three-spin system, strong pulses of 13 G yielded an extra peak around ~23 Å, which was diminished when using weaker pulses that flip only a fraction of the spins (Figure 2d). Therefore, in our further experiments we used 5.6 G pump pulse, which renders the three-spin effects negligible.

## Dynamic nature of the transport domain

We collected DEER data on 8 transport domain mutants in detergent and lipid membranes either in the apo state or bound to $Na^+$ and Asp or to TBOA, yielding 44 different samples. Very broad distance distributions, spanning up to 40 – 50 Å, were obtained for almost all samples, except in a few cases (Figure 3 and Supplementary Figures 4). In most of the detergent samples, additions of $Na^+$ and Asp or $Na^+$ and TBOA shifted the distributions mid points toward longer distances in the extracellular mutants (by an average of 2.2 and 4.3 Å, respectively) and toward shorter distances in the intracellular mutants (by ~2.8 and 3 Å, respectively). These systematic changes suggest that the broad distance distributions are not due to local flexibility but arise from $Glt_{Ph}$ protomers populating independently both the outward and inward facing states, and that binding of both Asp and TBOA in detergent favors the outward facing state to some extent. It is, in principle, possible that the distance distributions are due to the protomers sampling not only the fully outward and inward facing states, but the intermediate positions as well. Indeed, a recent crystal structure has captured a $Glt_{Ph}$ protomer in an intermediate orientation[9], suggesting that the energies of the intermediate states may not be prohibitively high. However, we think that the intermediates do not contribute to the conformational ensemble because the distributions obtained in the presence of TBOA are similarly broad. The benzyl group of TBOA is expected to prevent the occlusion of the inhibitor in the binding site, disabling translocation[7,36]. Therefore, the broad distributions must originate from the contributions of $Glt_{Ph}$ protomer pairs in discrete configurations. Modeling also showed that the experimental distance distributions could not be explained by a single conformation, since they covered the distances predicted for both states (Supplementary Figure 4). These observations suggest that in detergent solutions and in lipid bilayers both in the bound and unbound states, $Glt_{Ph}$ protomers are distributed between the outward and inward facing conformations.

## Conformational selection in the lipid bilayer

Overall, distance distributions were similarly broad in detergent micelles and in lipid bilayers. However, there were several exceptions, including K290R1 bound to TBOA,

E296R1 in either apo or bound states, and A364R1 bound to Asp, for which the distributions were broad in detergent, but narrow in the bilayers. Particularly for residue 296, we observed very narrow peaks, indicative of steric constraints on R1 mobility. The distribution medians in the bilayers were consistent with the outward orientation of the intracellular mutants K290R1 and E296R1, and inward orientation of the extracellular mutant A364R1. Interestingly, the crystal structures suggest that these residues are not in a direct contact with the lipid in either the outward or inward facing states. If so, than why do the R1 side chains stabilize specific states in lipid bilayers and not in detergents? The intracellular residues 290 and 296 are located on the interface between the transport and trimerization domains in the outward facing state, where they are well positioned to participate in the inter-domain interactions. In contrast, they are distant from the interface in the inward facing state. The opposite is true for residue 364, which is adjacent to the trimerization domain lysine 55 in the inward but not outward facing state. Hence, we hypothesize that the nitroxide side chains, which possess both the hydrophobic character and the hydrogen bond acceptor potential, are engaged into the inter-domain interactions, and that the favorable energetic contributions of such interactions are larger in the context of the bilayer compared to detergent micelles. Interestingly, for residue 364 we observe stabilization of the inward facing state in membranes only in complex with Asp but not TBOA. Consistently, in the crystal structure of the TBOA-bound $Glt_{Ph}$, HP2 is in an open conformation and residue 364 is distant from the domain interface.

## Quantitative analysis of the distance distributions

Because the broad experimental distributions suggested that both outward and inward facing states were present, we aimed to determine their populations. Computational predictions based on R1 rotamer libraries yielded average distances that agreed well with the experiment (Supplementary Table 1), but the predicted and experimental distance distributions differed substantially. Hence for quantitative analysis, we modeled the experimental data as sums of three Gaussian functions, representing the distance distributions originating from possible configurations of the subunit pairs: both outward, both inward, and mixed, i.e. one outward and one inward. Assuming that the protomers isomerize between the outward and inward facing states independently of each other, and taking the probability of a protomer to be in the outward facing state as $p_O$, the probabilities of the two neighboring subunits facing outward or inward are $p_O{}^2$ and $(1 - p_O)^2$, respectively, and the probability that they are in the mixed configurations is $2p_O(1 - p)$). Notably in mixed configurations, the distances from outward to inward and from inward to outward protomers are not quite the same, as the transport domain movements combine translation and rotation. Nevertheless, we represented them as a single Gaussian, because increasing the number of the optimized parameters was statistically unjustified. The distance probability, $P(r)$, is then:

$$P(r) = S \cdot \left( \frac{p_O^2}{\sigma_O} G_O + \frac{2p_O(1-p_O)}{\sigma_M} G_M + \frac{(1-p_O)^2}{\sigma_I} G_I \right) \quad (1)$$

where $G_O$, $G_M$, $G_I$ and $\sigma_O$, $\sigma_M$ and $\sigma_I$ are the Gaussian means and standard deviations for the outward, mixed and inward configurations, respectively; and $S$ is a normalization factor. The areas of the Gaussians are proportional to the configurations probabilities. As initial guesses

for the Gaussian means, we used either $C_\beta$-$C_\beta$ distances or distances derived from modeling, which we then optimized locally in the parameter space. During the fitting process, we generally constrained the Gaussian widths to less than 6 Å, an approximate upper limit for the distance distributions measured for structured residues[30–32]. The majority of the Gaussians satisfied this criterion, with a few exceptions when broader widths had to be used to adequately represent the distributions (Supplementary Table 1). The resulting fits described well both the distance distributions (Figure 3) and the time domain raw data (Supplementary Figure 5a). To verify the robustness of the data analysis and fitting, we varied the baseline, subtracted from the time domain data, which gave negligible variations (Supplementary Figure 6b, Supplementary Table 2 and Supplementary Note).

## Distances are consistent with the crystal structures

From the Gaussian fits, we extracted 139 distances, which were overall in excellent agreement with the $C_\beta$-$C_\beta$ distances and with distances calculated from the rotamer libraries (Figure 4a and Supplementary Table 1), yielding root mean square deviations (RMSD) of ~6 Å. Notably, 20 distance measurements between residues in T4 lysozyme[31] yield RMSD of 6.9 Å, suggesting that these values reflect the inherent differences between the $C_\beta$-$C_\beta$ distances and those between the paramagnetic atoms of R1. Interestingly, RMSDs calculated for the subsets of distances attributed to the symmetric outward and inward facing configurations were 5.5 and 6.8 Å, respectively, showing that DEER data were similarly consistent with the structures of the outward and inward facing conformations (Figure 4b). Also similar RMSDs were obtained for the measurements conducted in lipids and in detergent. However on average, distances in lipid bilayers were shorter than in detergent, suggesting that the overall protein structure was more compact (Figure 4c). Finally, the RMSDs for the apo, Asp- and TBOA-bound $Glt_{Ph}$ mutants in detergent were 6.2, 5.9 and 5.9 Å, respectively, and in lipid: 5.6, 4.7 and 6.3 Å (Figure 4d), suggesting that no structural re-arrangements involving the labeled residues took place that would be incompatible with the crystal structures.

The Gaussian means for the symmetric outward and inward facing configurations are scattered about the crystallographic $C_\beta$-$C_\beta$ distances with a small bias toward longer distances (Figure 4a–d). Such bias is typically observed for globular proteins, in which the R1 side chains are more likely to point away from the protein and from each other[37]. We also detect several outliers, for which the predicted and measured distances differ by as much as 8 – 15 Å (Supplementary Table 1). In three cases (residues 294, 364 and 378 in the inward facing state), the distances predicted from the rotamer libraries are in much better agreement with the experimental distances, possibly reflecting an underlying selection of specific rotamers. In other cases, modeling cannot explain the deviations, which may still be due to the selection of specific rotamers, reflect local structural flexibility, or point toward deviations from the crystal structures. When mapped onto the protein structures, most of the outliers with longer distances are observed on the extracellular side in the outward facing state and on the cytoplasmic side in the inward facing state (Figure 4e). In contrast, outliers with shorter distances all fall onto the extracellular side of the inward facing transporter. In the latter case, the residues are part of a sterically crowded environment possibly selecting for the R1 rotamers that point toward each other. Interestingly, it has been shown for a

mammalian homologue that the transport domains approach each other to within disulfide bond distances[38], perhaps reflecting a greater mobility range than suggested by the crystal structures. For the longer than expected distances, we note that several corresponding distance distributions are very broad, and hence are more consistent with the local flexibility of the protein backbone (Figure 4e and Supplementary Table 1).

### The states are nearly equienergetic

Fitted values of the outward facing state probabilities vary substantially between mutants. However on average, they fall between 0.4 and 0.8 for all ligand conditions and hydrophobic environments (Figure 5a), suggesting that the outward and inward facing states are similarly populated and hence, are similar in energy. Importantly, we find that three Gaussian functions with areas weighted by the binomial coefficients describe the data well, consistent with the individual protomers within $Glt_{Ph}$ trimer sampling conformational states independently of each other. Although our measurements cannot exclude subtle coupling between the subunits, we note that all or none transitions, such that the subunits are either all outward or inward facing, are neither required nor prohibited. Instead, we see a range of distributions. In some, the symmetrical states are dominant, while in others the mixed states are substantially populated. These results are in agreement with the previous functional experiments, postulating independence of the subunits within $Glt_{Ph}$ and the mammalian glutamate transporters[14,39–41]. On average, Asp and more so TBOA binding modestly shifted the distributions toward the outward facing state. These results are consistent with our recent measurements showing that the outward and inward facing states have similar affinities for Asp, and that the former binds TBOA tighter (unpublished data).

The wide range of $p_O$s obtained for various mutants may in part originate from the uncertainties of the fitting process. However, at least some of the differences can be understood from the structures, such as for the mutants on the domain interface in the lipid-reconstituted transporters discussed above. Others, such as a lower than average population of the outward facing state in $Glt_{Ph}$-T375R1 in detergent cannot be easily rationalized. Nevertheless, we note that the population change from 10 to 90 % corresponds to an energy difference of only 2.6 kcal/mol, a perturbation within the expectation for single residue mutations. Interestingly, all mutants have shown some level of Asp uptake (Supplementary Figure 6), suggesting that shifting the energy balance between the outward and inward facing states does not abrogate transport.

## Discussion

In membrane transporters, transitions between the outward and inward facing states are the linchpin of the catalytic mechanism. These isomerizations occur both in the substrate-loaded and substrate-free transporters to complete the cycle (Figure 5b). Crystal structures of the wild type $Glt_{Ph}$ have pictured the protein in symmetric outward facing states[6,7]. The structure of the symmetric inward facing state was determined by trapping the transporter using mercury-mediated cross-linking of two cysteine residues placed on the domain interface[8] and later recapitulated in the absence of the cross-links[9]. These structures pictured the outward to inward transition involving a large-scale trans-membrane movement of the

transport domain. The data presented here is a demonstration that these domain motions occur in detergent solution and, importantly, in membranes. We further develop a more complete picture of the conformational ensemble of the transporter by showing that the outward and inward facing states have similar energies both when the transporter is fully loaded with $Na^+$ and Asp and empty. Our measurements are consistent with the lack of either positive or negative cooperativity between the subunits of the trimer, picturing $Glt_{Ph}$ as a system of three largely independent protomers sampling the outward and inward facing states. Importantly, $Glt_{Ph}$ originates from a hyper-thermophilic archaeon and normally functions at 100 °C, where it is expected to better match the kinetic properties of the mammalian glutamate transporters[10]. At present, we do not know what the state distributions are at these temperatures. Extrapolations based on the binding experiments suggest that $Na^+$ and Asp affinity for the outward facing state of $Glt_{Ph}$ is higher than that for the inward facing state at elevated temperatures (unpublished data), a property also reported for the mammalian homologues at physiological temperature[42]. Hence, in these systems the ligands will stabilize the outward facing conformation more substantially, than we have observed here.

The mechanisms by which lipid bilayers stabilize specific conformations of membrane proteins, thereby modulating their function, have been extensively scrutinized with particular emphasis on the role of the hydrophobic mismatch between the proteins and the bilayer and on specific interactions with lipids[43–45]. In GltPh, the structural studies suggest that the movements of the transport domain would result in remodeling of the transport domain interface with the surrounding membrane. Hence, it is unexpected that transferring $Glt_{Ph}$ from the dynamic detergent micelles into the relatively rigid lipid bilayers has only a modest effect on the conformational ensemble. We observe an increase of the outward facing state population of only ~10 – 20 % on average, corresponding to ~0.5 kcal/mol more favorable free energy in lipid compared to detergent (Figure 5). However, the effects of the lipid environment are more pronounced in several mutants, including E296R1, A364R1 and K290R1, where we see single dominant conformations in lipids. The observed population shifts cannot be attributed to R1 side chains interacting with the lipid or detergent directly. Instead, they can be rationalized in terms of R1 interactions on the interface between the transport and trimerization domains, which become more favorable in membranes. This opens an interesting possibility that intra- and inter-protomer bond formation in membrane proteins may be more favorable in lipid bilayers than in more disordered detergent micelles. Consistently, a greater contribution of the inter-protomer hydrogen bond to the stability of glycophorin A dimer in native membranes compared to detergent has been recently reported[46]. We also observe that the average distances in lipid are shorter than in detergent, suggesting that the overall protein structure is more compact, perhaps leading to greater constraints on the interfacial protein side chains, smaller loss of the conformational entropy upon bond formation, and hence more favorable free energies. Such effects may contribute to the repertoire of mechanisms by which the bilayer alters the energetics of membrane proteins.

Whether the closely matching energies of the outward and inward facing states is a general phenomenon in transporters remains to be elucidated. In a lactose permease LacY, the cysteine accessibility studies suggest that the apo transporter is predominantly inward facing

and that sugar binding favors the outward facing states[47]. However, similarly to our results, DEER data on LacY showed that multiple conformations were populated under all ligand conditions[48]. Also, sodium and hydantoin symporter Mhp1 crystallized in both outward and inward facing conformations under similar conditions[49,50], suggesting that the two states were close in energy and well populated. Finally, theoretical considerations suggest that balancing the relative energies of the states would maximize the turnover rates[44]. Here we describe a robust method to probe state distributions of transporters under native-like conditions of the lipid bilayers, which can be applied to a wide range of systems. Importantly, our approach opens a way to investigate whether and how the nature of the lipid environment affects the conformational selection, and to establish a correspondence between the relative energies of the outward and inward facing states and substrate transport rates. It would be important to investigate whether the thickness of the lipid bilayer, its fluidity or specific lipid composition affect the state distributions, as well as to probe whether these membrane properties alter the strength of specific inter-domain interactions.

## Online Methods

### Molecular biology and protein purification

Cysteine mutations were introduced within cysteine-less seven histidine $Glt_{Ph}$ variant[8] using standard techniques and verified by DNA sequencing. All mutants were expressed and purified as described previously[6]. Briefly, C-terminal $(His)_8$ fusion constructs were expressed in *E. coli* DH10B cells (*Invitrogen, Inc*.) and purified by metal affinity chromatography. The tag was removed by thrombin digestion and the proteins were further purified by size exclusion chromatography. The final protein concentration of trimers was 15 – 30 μM, calculated from the absorbance at 280 nm using coefficient of 26, 820 $M^{-1}$ $cm^{-1}$ (per monomer). Samples were stored at −80 °C and further manipulated in buffer A containing in mM 20 HEPES, pH 7.4, 100 NaCl, 0.1 Asp, 1 DDM.

### Spin-labeling and DEER sample preparation

All mutants were spin-labeled with MTSL (*Toronto Research Chemicals*) in buffer A. MTSL was first dissolved in acetonitrile and added to the protein solutions in 20 – 30 fold (per monomer) molar excess. The labeling was performed for 3 hours at room temperature and continued overnight at 4 °C with agitation. The unreacted label was removed by dialysis against four changes of 30 ml buffer A over 30 hours using 25 kDa molecular weight cutoff membrane. To prepare substrate-free $Glt_{Ph}$, buffer B, containing in mM 20 HEPES, pH 7.4, 100 KCl, 1 DDM, was used during the last two buffer changes. When apo protein samples were prepared for further reconstitution into the bilayers, buffer B was supplemented with 2.5 mM NaCl. TBOA-bound protein was prepared starting with apo protein by adding NaCl and TBOA (*Tocris Bioscience*) to 50 mM and 125 μM, respectively. $Glt_{Ph}$ mutants were reconstituted into POPC (*Avanti Polar Lipids*) membranes at protein to lipid molar ratio of 1:2400 in DDM-free buffer A or buffer B, containing 2.5 mM NaCl. Aliquots of chloroform-solubilized POPC were dried under vacuum and re-hydrated at 50 mM using appropriate buffers. The lipid bilayers were destabilized by the addition of Triton-100 to the final lipid:Triton-100 ratio of 1:0.6 (w:w), and incubated with protein for 1 hr at room temperature. Pre-washed Bio-Beads (*Bio-Rad, Inc*.) were equilibrated in the appropriate

buffer, added to the mixtures of protein and lipid at 100 mg/ml, and incubated at room temperature for 2 hr. The beads were replaced twice and incubated with liposome suspensions for 4 hr at 4 °C. The multilayer vesicles were harvested by centrifugation at 70 000 g for 15 min. The vesicles containing apo $Glt_{Ph}$ were additionally washed three times by loading with DDM-free buffer B using freeze and thaw procedure followed by centrifugation. To prepare TBOA-bound lipid-reconsituted samples, the vesicles were washed in the same manner in buffer supplemented with NaCl and TBOA at 50 mM and 125 μM, respectively. The final concentration of the spin-labeled $Glt_{Ph}$ trimer in both DDM and POPC samples was 10 – 55 μM, based on the standard calibrated measurement of the primary echo amplitude, which gives total spin concentration. The reference sample was 200 μM 4-hydroxy-2,2,6,6-tetramethylpiperidin-1-oxyl (TEMPOL) in 50 w/v Glycerol-d8/$D_2O$[25]. The final $Glt_{Ph}$ trimer to lipid molar ratio was 1:2400, and lipid concentration was ~75 mg/ml. All samples were prepared in the final buffer containing 90 % $D_2O$ with protein samples in DDM also supplemented with Glycerol-d8 at 20% (w/v). Samples were loaded into 1.8 mm internal diameter capillary EPR tubes, and shock-frozen in liquid $N_2$. Samples were prepared and measured at least twice.

## DEER measurements

Measurements were performed at 60 K as previously described[32] using a 17.3 GHz home-built Ku-band pulse spectrometer[51], which has provided high sensitivity measurements in numerous previous studies[18,19,22–26,32,34,52]. A standard 4-pulse DEER sequence[53] with π/2-π-π pulse widths of 16, 32 and 32 ns, respectively, and a 32 ns π pump pulse was used routinely. When testing the three-spin effects, a 14 ns pump pulse with varied flip angles was used (Supplementary Note). The frequency separation between detection and pump pulses was 70 MHz. The detection pulses were positioned at the low-field edge of the nitroxide spectrum. Typical dipolar evolutions times were 1.5 to 5 μs as needed with signal averaging from 2 to 20 hours. The homogeneous background was removed from the raw time-domain signals and the distances were reconstructed from the baseline-corrected and normalized signals by using Tikhonov regularization method[54] and refined by Maximum Entropy Method (MEM) (Supplementary Note)[55].

## Modeling of distance distributions and data analysis

To model expected distance distributions, we used rotamer libraries generated by molecular modeling software MMM[33]. The ensembles of statistically weighed spin-label conformers were calculated at 175 K. The crystal structures of $Glt_{Ph}$ in the outward facing conformation with substrate (pdb 2NWX) or TBOA (pdb 2NWW) and inward facing conformation with substrate (pdb 3KBC) were used as templates for the calculations. In addition, we generated a structural model containing two protomers in the outward and one protomer in the inward facing conformation. The model construction was straightforward, because the conformations of the trimerization domains are similar in the outward and inward facing states, and there are no steric clashes. For the mixed states, we calculated the average distance distributions from outward to inward and from inward to outward protomers. The experimental distance distributions were fitted to a single Gaussian for residues in the trimerization domain and to a scaled sum of three Gaussians for residues in the transport domain using non-linear curve fitting algorithm within OriginLab software (*OriginLab*,

*Inc*.). As initial guesses for the Gaussians means, we used the average distances calculated by MMM, or the $C_\beta$-$C_\beta$ distances in the crystal structures and the structural model.

### Activity assay

For the transport activity measurements, spin-labeled and unlabeled $Glt_{Ph}$ mutants were reconstituted in POPC liposomes at protein to lipid ratio of 1:100 as previously described[7,10]. Porteoliposomes were loaded with buffer containing in mM 20 HEPES, pH 7.4, 100 KCl and 200 choline chloride, extruded through 0.4 μm nitrocellulose filters and incubated for 2 minutes at 30 °C in buffer containing in mM 20 HEPES, pH 7.4, 100 KCl, 200 NaCl and 600 nM $^3$H-L-aspartate. The uptake reactions were terminated by diluting proteoliposomes into ice-cold buffer, vesicles were harvested by filtration, and retained radioactivity was measured[7,10].

## Supplementary Material

Refer to Web version on PubMed Central for supplementary material.

## Acknowledgements

The work was supported by US National Instituted of Neurologic Disorders and Stroke grants NS064357 and NS064357-02S1 to O.B. and grants US National Center for Research Recourses grant P41-RR016292, US National Instituted of Neurologic Disorders and Stroke grant P41GM103521 and US National Institute of Biomedical Imaging grant R010EB003150 J.H.F.

## References

1. Danbolt NC. Glutamate uptake. Prog Neurobiol. 2001; 65:1–105. [PubMed: 11369436]
2. Hinoi E, Takarada T, Tsuchihashi Y, Yoneda Y. Glutamate transporters as drug targets. Curr Drug Targets CNS Neurol Disord. 2005; 4:211–20. [PubMed: 15857305]
3. Levy LM, Warr O, Attwell D. Stoichiometry of the glial glutamate transporter GLT-1 expressed inducibly in a Chinese hamster ovary cell line selected for low endogenous Na+-dependent glutamate uptake. J Neurosci. 1998; 18:9620–8. [PubMed: 9822723]
4. Zerangue N, Kavanaugh MP. Flux coupling in a neuronal glutamate transporter. Nature. 1996; 383:634–7. [PubMed: 8857541]
5. Owe SG, Marcaggi P, Attwell D. The ionic stoichiometry of the GLAST glutamate transporter in salamander retinal glia. J Physiol. 2006; 577:591–9. [PubMed: 17008380]
6. Yernool D, Boudker O, Jin Y, Gouaux E. Structure of a glutamate transporter homologue from Pyrococcus horikoshii. Nature. 2004; 431:811–8. [PubMed: 15483603]
7. Boudker O, Ryan RM, Yernool D, Shimamoto K, Gouaux E. Coupling substrate and ion binding to extracellular gate of a sodium-dependent aspartate transporter. Nature. 2007; 445:387–93. [PubMed: 17230192]
8. Reyes N, Ginter C, Boudker O. Transport mechanism of a bacterial homologue of glutamate transporters. Nature. 2009; 462:880–5. [PubMed: 19924125]
9. Verdon G, Boudker O. Crystal structure of an asymmetric trimer of a bacterial glutamate transporter homolog. Nat Struct Mol Biol. 2012; 19:355–7. [PubMed: 22343718]
10. Ryan RM, Compton EL, Mindell JA. Functional characterization of a Na+-dependent aspartate transporter from Pyrococcus horikoshii. J Biol Chem. 2009; 284:17540–8. [PubMed: 19380583]
11. Groeneveld M, Slotboom DJ. Na+: aspartate coupling stoichiometry in the glutamate transporter homologue GltPh. Biochemistry. 2010; 49:3511–3513. [PubMed: 20349989]

12. Yernool D, Boudker O, Folta-Stogniew E, Gouaux E. Trimeric subunit stoichiometry of the glutamate transporters from Bacillus caldotenax and Bacillus stearothermophilus. Biochemistry. 2003; 42:12981–8. [PubMed: 14596613]
13. Gendreau S, et al. A trimeric quaternary structure is conserved in bacterial and human glutamate transporters. J Biol Chem. 2004; 279:39505–12. [PubMed: 15265858]
14. Groeneveld M, Slotboom DJ. Rigidity of the subunit interfaces of the trimeric glutamate transporter GltT during translocation. J Mol Biol. 2007; 372:565–70. [PubMed: 17673229]
15. Focke PJ, Moenne-Loccoz P, Larsson HP. Opposite movement of the external gate of a glutamate transporter homolog upon binding cotransported sodium compared with substrate. J Neurosci. 2011; 31:6255–62. [PubMed: 21508248]
16. Huang Z, Tajkhorshid E. Dynamics of the extracellular gate and ion-substrate coupling in the glutamate transporter. Biophys J. 2008; 95:2292–300. [PubMed: 18515371]
17. Shrivastava IH, Jiang J, Amara SG, Bahar I. Time-resolved mechanism of extracellular gate opening and substrate binding in a glutamate transporter. J Biol Chem. 2008; 283:28680–90. [PubMed: 18678877]
18. Borbat PP, Freed JH. Measuring distances by pulsed dipolar ESR spectroscopy: spin-labeled histidine kinases. Methods Enzymol. 2007; 423:52–116. [PubMed: 17609127]
19. Borbat PP, Freed JH. Pros and Cons of Pulse Dipolar ESR: DQC and DEER. EPR Newsletter. 2007; 17:21–33.
20. Mchaourab HS, Steed PR, Kazmier K. Toward the fourth dimension of membrane protein structure: insight into dynamics from spin-labeling EPR spectroscopy. Structure. 2011; 19:1549–61. [PubMed: 22078555]
21. Reginsson GW, Schiemann O. Pulsed electron-electron double resonance: beyond nanometre distance measurements on biomacromolecules. Biochem J. 2011; 434:353–63. [PubMed: 21348855]
22. Borbat PP, et al. Conformational motion of the ABC transporter MsbA induced by ATP hydrolysis. PLoS Biol. 2007; 5:e271. [PubMed: 17927448]
23. Tong J, Borbat PP, Freed JH, Shin YK. A scissors mechanism for stimulation of SNARE-mediated lipid mixing by cholesterol. Proc Natl Acad Sci U S A. 2009; 106:5141–6. [PubMed: 19251653]
24. Georgieva ER, Ramlall TF, Borbat PP, Freed JH, Eliezer D. Membrane-bound alpha-synuclein forms an extended helix: long-distance pulsed ESR measurements using vesicles, bicelles, and rodlike micelles. J Am Chem Soc. 2008; 130:12856–7. [PubMed: 18774805]
25. Georgieva ER, Ramlall TF, Borbat PP, Freed JH, Eliezer D. The lipid-binding domain of wild type and mutant alpha-synuclein: compactness and interconversion between the broken and extended helix forms. J Biol Chem. 2010; 285:28261–74. [PubMed: 20592036]
26. Upadhyay AK, Borbat PP, Wang J, Freed JH, Edmondson DE. Determination of the oligomeric states of human and rat monoamine oxidases in the outer mitochondrial membrane and octyl beta-D-glucopyranoside micelles using pulsed dipolar electron spin resonance spectroscopy. Biochemistry. 2008; 47:1554–66. [PubMed: 18198902]
27. Vamvouka M, Cieslak J, Van Eps N, Hubbell W, Gross A. The structure of the lipid-embedded potassium channel voltage sensor determined by double-electron-electron resonance spectroscopy. Protein Sci. 2008; 17:506–17. [PubMed: 18287283]
28. Claxton DP, et al. Ion/substrate-dependent conformational dynamics of a bacterial homolog of neurotransmitter:sodium symporters. Nat Struct Mol Biol. 2010; 17:822–9. [PubMed: 20562855]
29. Joseph B, Jeschke G, Goetz BA, Locher KP, Bordignon E. Transmembrane gate movements in the type II ATP-binding cassette (ABC) importer BtuCD-F during nucleotide cycle. J Biol Chem. 2011; 286:41008–17. [PubMed: 21953468]
30. Borbat PP, Mchaourab HS, Freed JH. Protein structure determination using long-distance constraints from double-quantum coherence ESR: study of T4 lysozyme. J Am Chem Soc. 2002; 124:5304–14. [PubMed: 11996571]
31. Kazmier K, Alexander NS, Meiler J, Mchaourab HS. Algorithm for selection of optimized EPR distance restraints for de novo protein structure determination. J Struct Biol. 2011; 173:549–57. [PubMed: 21074624]

32. Georgieva ER, et al. Effect of freezing conditions on distances and their distributions derived from Double Electron Electron Resonance (DEER): A study of doubly-spin-labeled T4 lysozyme. J Magn Reson. 2012; 216:69–77. [PubMed: 22341208]
33. Polyhach Y, Bordignon E, Jeschke G. Rotamer libraries of spin labelled cysteines for protein studies. Phys Chem Chem Phys. 2011; 13:2356–66. [PubMed: 21116569]
34. Bhatnagar J, et al. Structure of the ternary complex formed by a chemotaxis receptor signaling domain, the CheA histidine kinase, and the coupling protein CheW as determined by pulsed dipolar ESR spectroscopy. Biochemistry. 2010; 49:3824–41. [PubMed: 20355710]
35. Jeschke G, Sajid M, Schulte M, Godt A. Three-spin correlations in double electron-electron resonance. Phys Chem Chem Phys. 2009; 11:6580–91. [PubMed: 19639133]
36. Shimamoto K, et al. DL-threo-beta-benzyloxyaspartate, a potent blocker of excitatory amino acid transporters. Mol Pharmacol. 1998; 53:195–201. [PubMed: 9463476]
37. Bhatnagar J, Freed JH, Crane BR. Rigid body refinement of protein complexes with long-range distance restraints from pulsed dipolar ESR. Methods Enzymol. 2007; 423:117–33. [PubMed: 17609128]
38. Jiang J, Shrivastava IH, Watts SD, Bahar I, Amara SG. Large collective motions regulate the functional properties of glutamate transporter trimers. Proc Natl Acad Sci U S A. 108:15141–6. [PubMed: 21876140]
39. Grewer C, et al. Individual subunits of the glutamate transporter EAAC1 homotrimer function independently of each other. Biochemistry. 2005; 44:11913–23. [PubMed: 16128593]
40. Koch HP, Larsson HP. Small-scale molecular motions accomplish glutamate uptake in human glutamate transporters. J Neurosci. 2005; 25:1730–6. [PubMed: 15716409]
41. Leary GP, Stone EF, Holley DC, Kavanaugh MP. The glutamate and chloride permeation pathways are colocalized in individual neuronal glutamate transporter subunits. J Neurosci. 2007; 27:2938–42. [PubMed: 17360916]
42. Zhang Z, et al. Transport direction determines the kinetics of substrate transport by the glutamate transporter EAAC1. Proc Natl Acad Sci U S A. 2007; 104:18025–30. [PubMed: 17991780]
43. Phillips R, Ursell T, Wiggins P, Sens P. Emerging roles for lipids in shaping membrane-protein function. Nature. 2009; 459:379–85. [PubMed: 19458714]
44. Andersen OS, Koeppe RE 2nd. Bilayer thickness and membrane protein function: an energetic perspective. Annu Rev Biophys Biomol Struct. 2007; 36:107–30. [PubMed: 17263662]
45. Lee AG. How lipids affect the activities of integral membrane proteins. Biochim Biophys Acta. 2004; 1666:62–87. [PubMed: 15519309]
46. Duong MT, Jaszewski TM, Fleming KG, MacKenzie KR. Changes in apparent free energy of helix-helix dimerization in a biological membrane due to point mutations. J Mol Biol. 2007; 371:422–34. [PubMed: 17570394]
47. Kaback HR, et al. Site-directed alkylation and the alternating access model for LacY. Proc Natl Acad Sci U S A. 2007; 104:491–4. [PubMed: 17172438]
48. Smirnova I, et al. Sugar binding induces an outward facing conformation of LacY. Proc Natl Acad Sci U S A. 2007; 104:16504–9. [PubMed: 17925435]
49. Weyand S, et al. Structure and molecular mechanism of a nucleobase-cationsymport-1 family transporter. Science. 2008; 322:709–13. [PubMed: 18927357]
50. Shimamura T, et al. Molecular basis of alternating access membrane transport by the sodium-hydantoin transporter Mhp1. Science. 2010; 328:470–3. [PubMed: 20413494]
51. Borbat PP, Crepeau RH, Freed JH. Multifrequency two-dimensional Fourier transform ESR: an X/Ku-band spectrometer. J Magn Reson. 1997; 127:155–67. [PubMed: 9281479]
52. Borbat, PP.; Freed, JH. Pulse dipolar ESR: distance measurements. In: Harmer, J.; Timmel, C., editors. Structural Information from Spin-Labels and Intrinsic Paramagnetic Centres in the Biosciences. Structure and Bonding. Springer; Berlin: 2012.
53. Pannier M, Veit S, Godt A, Jeschke G, Spiess HW. Dead-time free measurement of dipole-dipole interactions between electron spins. J Magn Reson. 2000; 142:331–40. [PubMed: 10648151]
54. Chiang YW, Borbat PP, Freed JH. The determination of pair distance distributions by pulsed ESR using Tikhonov regularization. J Magn Reson. 2005; 172:279–95. [PubMed: 15649755]

55. Chiang YW, Borbat PP, Freed JH. Maximum entropy: a complement to Tikhonov regularization for determination of pair distance distributions by pulsed ESR. J Magn Reson. 2005; 177:184–96. [PubMed: 16137901]

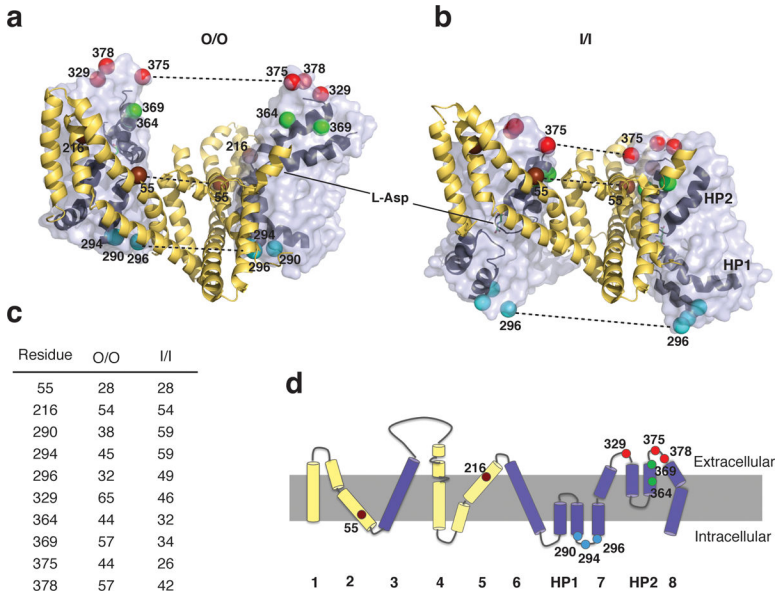


| Residue | O/O | I/I |
|---|---|---|
| 55 | 28 | 28 |
| 216 | 54 | 54 |
| 290 | 38 | 59 |
| 294 | 45 | 59 |
| 296 | 32 | 49 |
| 329 | 65 | 46 |
| 364 | 44 | 32 |
| 369 | 57 | 34 |
| 375 | 44 | 26 |
| 378 | 57 | 42 |

**Figure 1. Spin labeled residues**

(**a**) Pairs of $Glt_{Ph}$ protomers in the outward (O/O) and inward (I/I) facing states with the trimerization and transport domains shown in cartoon and transparent surface representations, respectively, and colored yellow and blue. For clarity, the third protomer is removed. The $C_\beta$ atoms of the residues, mutated to cysteines are shown as spheres and colored by region: trimerization domain, brown; intracellular side of the transport domain, blue; extracellular side of the transport domain, red; and HP2, green. (**b**) The $C_\beta$-$C_\beta$ distances listed for the mutated residues in symmetrical protomer pairs in the outward and inward facing states. (**c**) The topology of a $Glt_{Ph}$ protomer with positions of the spin-labeled residues highlighted as spheres and colored as in panel **a**.

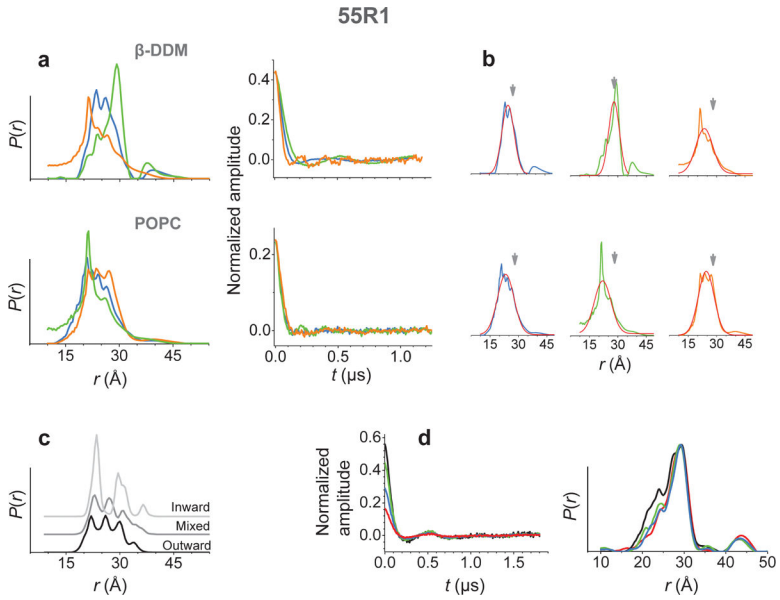


**Figure 2. Narrow distance distributions of the trimerization domain residue 55**

(**a**) The experimental data for K55R1 in detergent n-dodecyl-β-D-maltopyranoside (DDM) and in lipid 1-palmitoyl-2-oleoylphosphatidylcholine (POPC): the distance distributions (left) and the time domain data (right). The distance distributions were normalized to integral of unity and the y-axis corresponds to the distance probability, $P(r)$. The data for the apo $Glt_{Ph}$ and for the transporter bound to $Na^+$ and Asp, or $Na^+$ and TBOA are in blue, green and orange, respectively. (**b**) The experimental distances and single Gaussian approximations (red) for detergent (upper panel) and lipid (lower panel). The gray arrows at 28 Å correspond to $C_\beta$-$C_\beta$ distance in the crystal structures. (**c**) The distance distributions predicted from the rotamer libraries. (**d**) The time-domain data and distance distributions, respectively, obtained using pump pulse of 13 (black), 9.2 (green), 6.5 (blue) and 4.6 G (red).

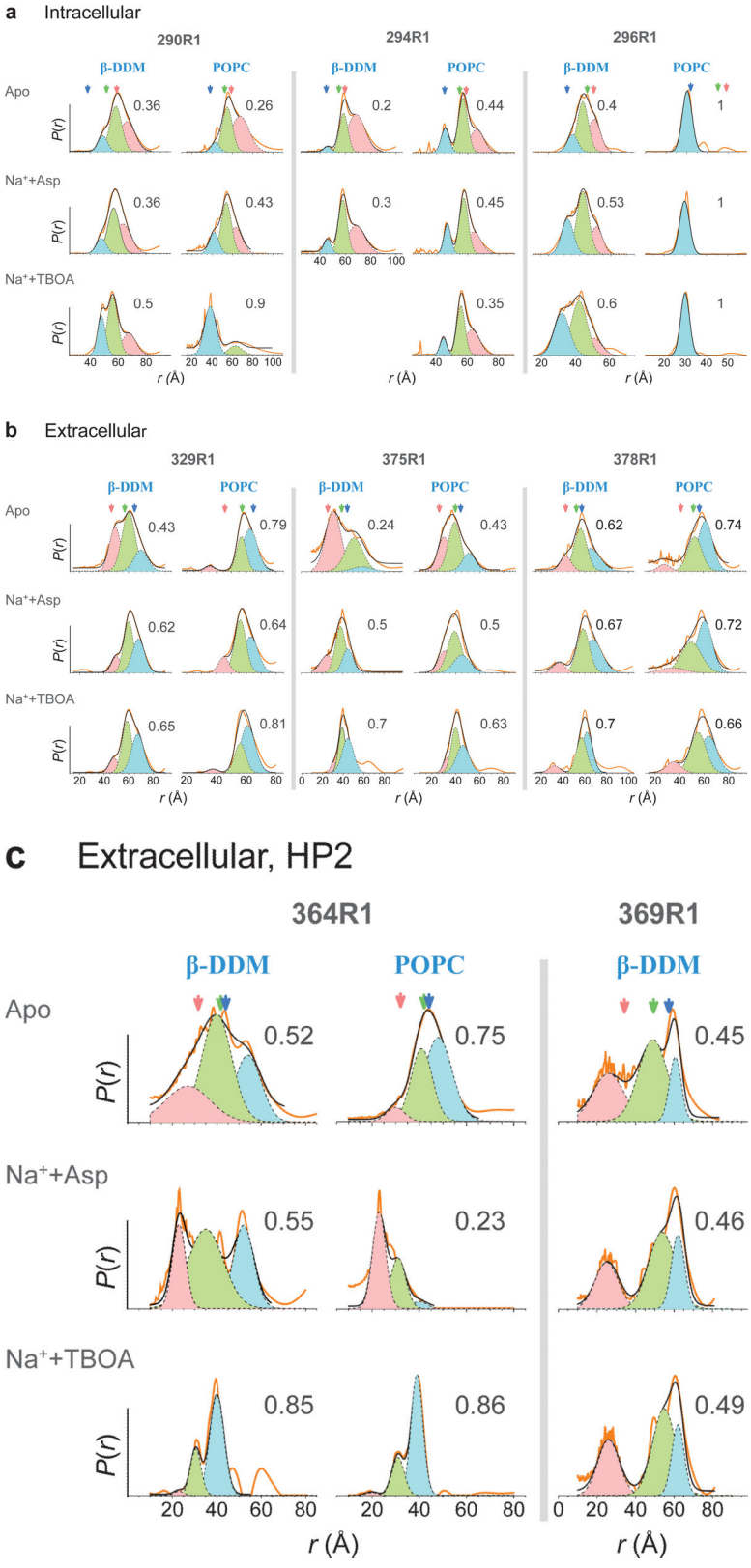


**Figure 3. Broad distance distributions measured for resides in the transport domain**

(**a,b**) Distance distributions for $Glt_{Ph}$ mutants in DDM solutions and POPC bilayer: (**a**) intracellular mutants K290R1, I294R1, and E296R1; (**b**) extracellular mutants L329R1, T375R1, and N378R1; and (**c**) HP2 mutants, A364R1 and S369R1. Orange and black lines show the experimental distance distributions and the envelope of the three fitted Gaussians, respectively. Gaussians representing distances from the symmetric outward, mixed and symmetric inward facing protomer configurations are shown in solid blue, green and pink, respectively. The arrows mark the $C_\beta$-$C_\beta$ distances, expected from crystal structures and are plotted in the same colors as for the Gaussians. The fitted populations of outward facing state, $p_O$, are shown next to the graphs.

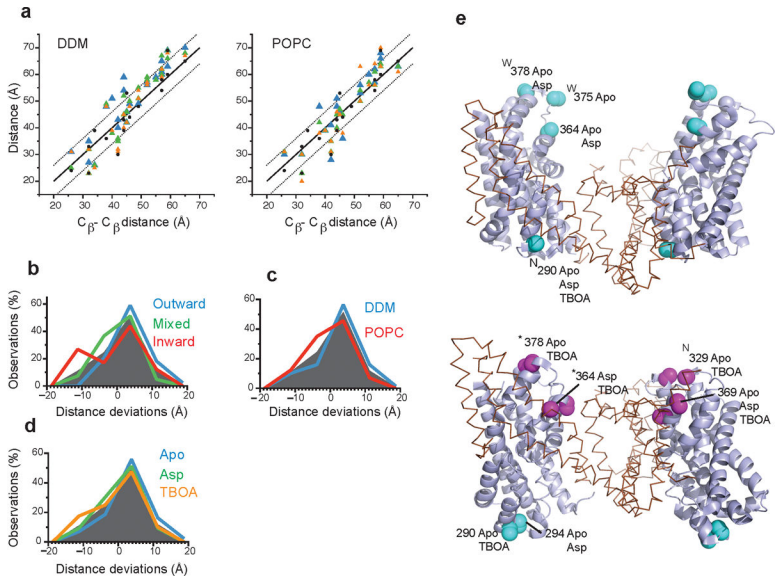


**Figure 4. Comparison between measured and expected distances**

(**a**) Comparison between the distances derived from the three Gaussian fits of the data in detergent (left) and lipid (right) and those measured between the $C_\beta$ atoms in the crystal structures. The data are plotted for apo, Asp- and TBOA-bound transporter as blue, green and orange triangles, respectively. The average values obtained using the rotamer libraries are shown as black circles. (**b–d**) The distributions of the distance deviations from panels **a** and **b** binned into 7.5 Å intervals for the entire dataset (grey shaded area) or for data grouped by (**b**) the protomer configuration: symmetric outward (blue), mixed (green) and symmetric inward (red); (**c**) environment: detergent (red) and lipid (blue); and (**d**) the added ligand: apo (blue), Asp- (green) and TBOA-bound (orange). (**e**) Residues showing distance deviations of at least 8 Å mapped onto the structure of $Glt_{Ph}$ protomer pairs in outward (top) and inward (bottom) configurations. The trimerization and transport domains are shown in ribbon and cartoon representations and colored brown and light blue, respectively. The Cα and $C_\beta$ atoms of the residues with shorter and longer distances are emphasized as spheres and colored magenta and cyan, respectively. The labels show the residue number and the ligand conditions under which the deviations are observed. The superscripts indicate those deviations, which are in a good agreement with the rotamer library predictions (star), or are associated with very wide (W) and narrow (N) distance distributions.

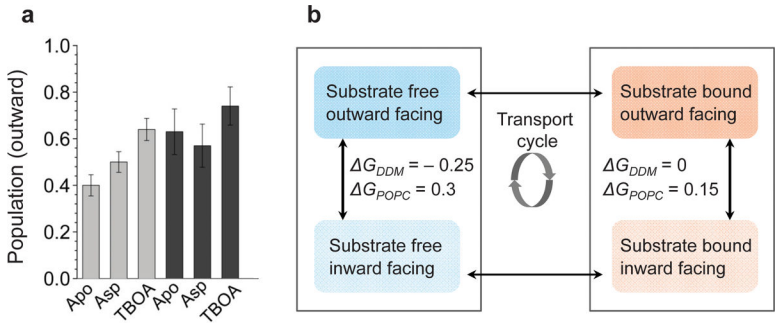


**Figure 5. The inward and outward facing states of $Glt_{Ph}$ are equienergetic**

(**a**) The average populations of the outward facing state and their standard errors, obtained from the Gaussian fits of the data collected in detergent (light gray bars) and in lipid (dark gray bars). The ligand conditions are shown underneath the bars. (**b**) The transport cycle chart with the estimated free energies (kcal/mol) of the transitions from the outward to inward facing conformations.